Classical Monte-Carlo simulations of X-ray-induced electron cascades in various materials

Vladimir Lipp[a], Nikita Medvedev[b,c], and Beata Ziaja[a,d]

[a]Center for Free-Electron Laser Science, DESY, 22607 Hamburg, Germany
[b]Institute of Physics, Academy of Science of Czech Republic, Na Slovance 1999/2, 18221 Prague 8, Czech Republic
[c]Institute of Plasma Physics, Academy of Science of Czech Republic, Za Slovankou 1782/3, 18200 Prague 8, Czech Republic
[d]Institute of Nuclear Physics, Polish Academy of Sciences, Radzikowskiego 152, 31-342 Krakow, Poland

ABSTRACT

In this paper, we present an extension to our code, XCASCADE [Medvedev, Appl. Phys. B 118, 417], that enables to model time evolution of electron cascades following low-intensity X-ray excitation in various materials consisting of elements with atomic numbers $Z = 1 - 92$. The code is based on a classical Monte-Carlo scheme and uses atomistic cross sections to describe electron impact ionization. The new extended version, XCascade-3D, also tracks the electron trajectories with 3D spatial resolution. This model takes into account anisotropic scattering of electrons on atoms. We show that the calculated electron ranges in various materials are in a good agreement with the available data, confirming the potential for high accuracy applications at FEL pulse diagnostics.

Keywords: Classical Monte Carlo, electron cascades, X-ray-induced electron kinetics, Free-electron lasers, XCASCADE, XCascade-3D, computer simulation, electron ranges

1. INTRODUCTION

X-ray pulse triggers a sequence of processes in an irradiated target,[1] including photoabsorption by deep-shell and valence electrons, Auger decays, fluorescence and secondary electron cascades. Electron-lattice energy exchange, mediated by electron-phonon coupling, leads at later stages to the heating of the lattice. All these processes finally can result in observable material modifications such as, e.g., atomic relocations, defect creation etc.

X-ray pulses generated with modern free-electron lasers (FEL)[2–6] find numerous applications, from nanostructuring[7] to imaging.[8] In order to achieve high accuracy in the corresponding measurements and simulations a precise diagnostics of the pulses is necessary. Recently, we developed an in-house Monte Carlo (MC) tool, XCASCADE,[9] that provides temporal information about FEL-induced electron cascades, such as cascading time and time-resolved carrier density. This simulation tool has already been successfully applied for diagnostics of single-shot pulse duration and arrival times of FELs,[10,11] using X-ray pump-optical probe scheme.

In addition to the temporal information, a spatial characteristics of FEL pulses might be required in some experiments. There are a few techniques aiming at it, e.g., utilizing FEL-induced defects (color centers) in alkali halides for spatial characterization of the pulse.[12,13] Formation of such temporally stable point defects may allow to extract pulse shape information in post-mortem measurements.

Email: vladimir.lipp@desy.de

Damage to VUV, EUV, and X-ray Optics VI, edited by Libor Juha, Saša Bajt, Regina Soufli, Proc. of SPIE Vol. 10236, 102360H · © 2017 SPIE · CCC code: 0277-786X/17/$18 · doi: 10.1117/12.2267939

In this report, we present an extension to the XCASCADE code, XCascade-3D, which provides full 3D-resolved information about FEL-induced electron cascades, induced by low-intensity X-ray pulse. By low-intensity pulse we understand the pulse which excites low number of electrons in total so that: (i) the approximation of non-interacting electron cascades independently developed in (ii) semi-neutral medium holds with sufficient accuracy. In sec. 2, we explain how our model is constructed and discuss its limits of applicability. In sec. 3 we study the influence of the effective energy gap on the model results. Sec. 4 is devoted to model testing; we show that averaging over 10 000 trajectories is enough to provide a sufficient statistical accuracy and discuss the dependence of the electron ranges on the angular scattering scheme. Finally, in sec. 5 we show on the examples of silicon, gold, and polystyrene that the model predictions are in a good agreement with the available data on electron ranges in various materials.

2. THE MODEL

XCASCADE uses an event-by-event Monte Carlo scheme, which is widely applied to follow electron cascades.[14,15] In this section we only briefly describe the simulation scheme. More details can be found in the previous publication devoted to XCASCADE.[9]

The material structure is assumed to be a homogeneous bulk of atomic/molecular density corresponding to the density of the modeled material. It allows us to utilize the Poisson distribution for sampling mean free paths of particles in matter. Atomic cross sections are applied to model the photon absorption and the electron-atom scattering within the material. Such approximation is justified for high-energy X-rays and for high-energy electron-atom collisions, since they excite electrons from the deeply lying core levels. However, this description neglects collective effects, such as the influence of band structure. The latter can be substantial at lower electron impact energies. In order to overcome this limitation for low-energy collisions, we introduce an effective excitation energy, replacing the bound levels in the valence band by a single 'effective' energy level, or an 'effective' band gap (similarly to the idea from Ref.[16]). In sec. 3, we explain how the effective energy gap values are chosen for different materials and demonstrate the advantage of this correction.

An electron cascade starts when an X-ray photon excites a photoelectron and creates an inner-shell hole in an atom of the target. A choice of the photabsorbing shell is made upon the relative photoabsorption cross section, extracted from the EPDL97 database.[17] A part of the photon energy is used to release a bound electron from valence level or a deep-shell hole; the rest contributes to the kinetic energy of the photoelectron. The binding energies are taken from the EADL database.[18] The trajectory of an energetic electron (photoelectron, incident electron, or secondary electron) is modeled as a straight line until an elastic scattering on an atom or an inelastic collision with an atom (here, always with impact ionization) occur. In our scheme, the elastic collisions influence only the direction of the propagating electron. During the inelastic collisions, the electron, in addition to the changing the direction, loses energy to excite secondary electrons. The probabilities of collisions, the energy losses of the electrons, and the scattering angles are calculated with the atomistic cross sections.

The created deep-shell hole can undergo either an Auger or a radiative decay (with the corresponding lifetimes[19]). For light elements the predominant decay channel is single Auger decay, during which the excess energy from the hole relaxation is used to create another secondary electron (Auger electron).[20] For heavier elements, many-step Auger decays may occur, resulting in several additional valence holes and free electrons.

In our model, the cascading stops when the energies of all electrons fall below 10 eV, i.e., when the electron scatters mostly elastically. Such cascade can last up to hundreds of femtoseconds, depending on the initial photon energy and the material properties.[9] Classical Monte Carlo averages over many trajectories providing statistically reliable results. The dependence of results on the number of iterations will be discussed below.

The electron mean free path is inversely proportional to the cross section of scattering.[14] Thus, the cross sections are the crucial parameters of the model. The inelastic cross sections are calculated with the binary-encounter-Bethe (BEB) model,[9,21] i.e., as discussed above, we assume that the material consists of non-interacting atoms.

For the elastic collisions, we apply Mott's cross section:[22]

$$\sigma_{el} = \frac{\pi Z(Z+1)r_e^2}{\eta(\eta+1)}\frac{1-\beta^2}{\beta^4}, \tag{1}$$

where Z is the atomic number, r_e is the classical electron radius, $\beta = v_e^2/c^2$ with v_e denoting the velocity of the electron, and c denoting the speed of light in vacuum. The empirically modified Moliere's screening is:[23]

$$\eta = \frac{1}{4}\left(\frac{\alpha c}{0.885 v_e}\right)^2 Z^{2/3}\left[1.13 + 3.76(\alpha Z/\beta)^2\left(\frac{\tau}{\tau+1}\right)^{1/2}\right]. \tag{2}$$

Here, α is the fine structure constant, m_e is the free electron mass, and τ is the kinetic energy of the electron in the units of its rest energy.

Fig. 1 shows the elastic and inelastic cross sections used in XCascade-3D on the example of silicon and gold.

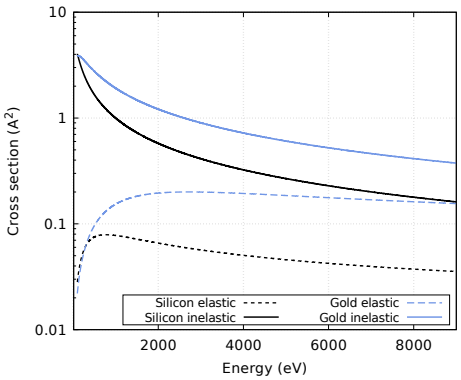

Figure 1.
Elastic (Eq. (1), dashed lines) and inelastic[21] (solid lines) cross sections for scattering of impact electron on silicon and gold atoms used in the Xcascade-3D model.

The model enables to assume various scattering schemes: forward scattering, isotropic scattering and anisotropic scattering. The latter is implemented using the following choice of the scattering angle:[24]

$$\cos(\chi) = 1 - \frac{2r(1-\xi)}{1+\xi(1-r)}, \tag{3}$$

where r is a random number uniformly distributed between $[0,1]$; parameter $\xi = 4\varepsilon/(1+4\varepsilon)$ corresponds to a case of the screened-Coulomb interaction with $\varepsilon = E/E_0$ a kinetic energy of the electron in atomic units ($E_0 = 27.21$ eV is the atomic energy unit). This approach captures the important feature of the process: The scattering is mostly isotropic for low-energy electrons, whereas at high energies impact electrons preferably scatter in the forward direction.[24] Although Eq. (3) was derived for elastic scattering, we will also utilize it for inelastic events as the simplest approximation. The direction of a secondary electron obeys the momentum conservation law. The azimuthal angle of scattering is chosen uniformly within the range of $[0, 2\pi)$.

As other transport Monte Carlo codes, the XCascade-3D scheme assumes that the fluence of the X-ray pulse is low. Consequently, we can neglect double excitations of the atoms by FEL photons. This also allows to neglect the band structure and electron-electron correlation effects within the excited electron ensemble: interaction between the excited electrons, and the Pauli blocking.[25] That assumption holds under the condition that the maximal achieved electron densities are much lower than the atomic densities of the target (less than $\sim 10^{21}$ cm^{-3}). The target is then assumed to be always undamaged and unexcited. Correspondingly, cross sections and rates for neutral material are used. Any shift of core levels in the modeled solids in respect to the corresponding atomic levels is neglected, since it introduces an error of several eV. In addition, all electrons considered are nonrelativistic.

3. MODEL PARAMETRIZATION

The only free parameter in our model is the effective energy gap. As we mentioned above, we use it to approximately account for the material's band structure (within the valence band) while using atomic binding energies for core levels. As we discussed earlier, we replace the valence electron binding energies in the target by a single effective energy level (effective band gap for semiconductors). This energy level is adjusted in such a way that the average electron-hole pair creation energy in the material equals to twice its band gap width. Such choice naturally fulfills the condition that the thresholds for impact ionizations by both electrons and holes are equal to the band gap,[16] similar to the empirical rule.[26]

We estimate the pair creation energy as the ratio between the energy of the absorbed photon and the total number of excited electrons by the end of the simulation, which started with the initial photoionization event. As an example, Fig. 2 shows the dependence of the predicted pair creation energy on the value of the effective band gap in silicon for 9 keV photons. Applying a linear fit, we could identify a value of the 'effective' band gap for silicon that corresponds to pair creation energy equal to twice the band gap, namely 1.79 eV. To the best of our knowledge, there is no experimental data on the band gap of polystyrene; we used 8.42 eV for the effective energy gap in this material. Note, that for metals we cannot introduce an effective band gap in such a way, therefore, for gold we use the atomic energy levels.

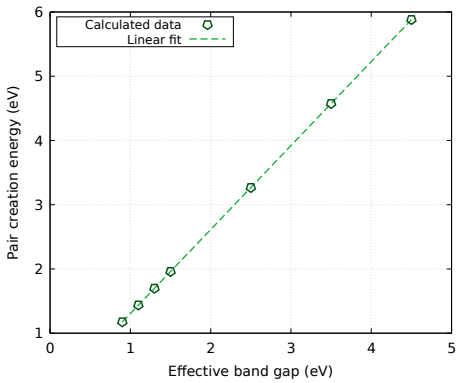

Figure 2. Pair creation energy obtained from our simulations as a function of the effective band gap in silicon.

4. MODEL TESTING

Fig. 3 presents a couple of typical cascades in silicon in real space projected onto the (XZ) plane. Each circle represents an event: yellow circle shows a site where the photon was absorbed (the origin of the cascade), blue circles show sites of core hole decays, green circles the sites of elastic scattering.

Red circles show the sites where inelastic collisions occurred. The photoelectron travels a certain distance in the material, undergoing elastic and inelastic collisions and creating deep-shell holes, until its energy falls below the threshold of 10 eV. Fig. 3 shows various branches of the electron cascades generated after a single photoabsorption.

In the following, we will calculate electron ranges in a few chosen materials. We define an electron range for each particular electron energy as the distance between the point where the impact electron entered the material and the point which it reached when its energy decreased to 10 eV. Thus, the range results directly from a MC simulation, avoiding the often-used continuous-slowing-down approximation.

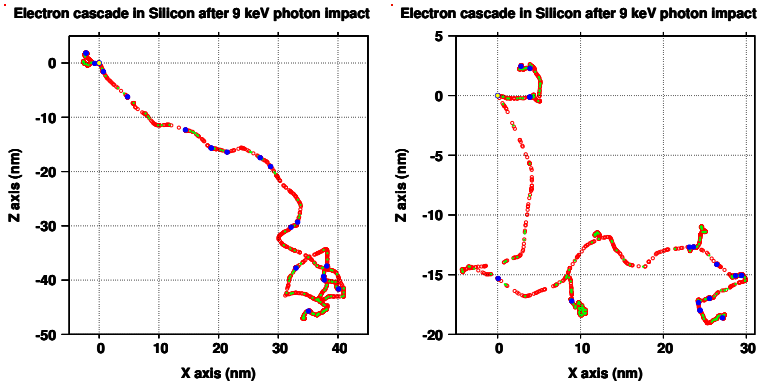

Figure 3. Examples of electron cascades in silicon.

Prior to the calculation, we study how the resulting electron ranges converge for various number of cascades. The examples of two photon energies: 200 eV and 20 keV, are shown in figure 4. One can see from Fig. 4 that for both cases approximately 10 000 cascades are needed to reach the relative accuracy of 0.5%. Therefore, in the following simulations we use around 10 000 cascades for estimating the electron range.

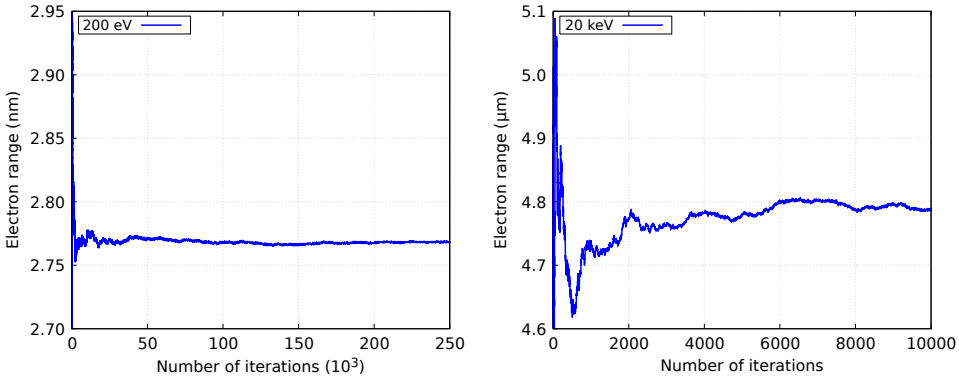

Figure 4. Convergence study of the electron range for silicon irradiated with 200 eV (left) and 20 keV (right) photon.

Fig. 5 presents a comparison of the electron ranges in silicon obtained with three scattering schemes: forward scattering (red dotted line), isotropic scattering (green dashed line), and anisotropic scattering (using Eq. (3), blue solid line). Notice that, in agreement with Eq. (3), at higher electron

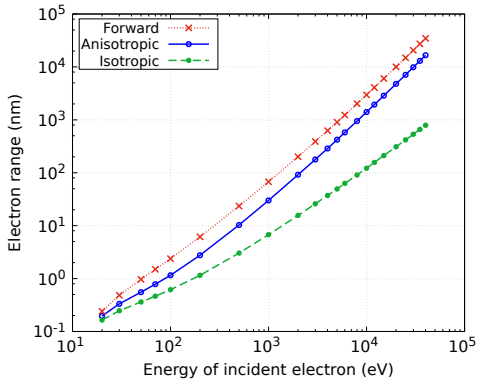

Figure 5. Electron ranges in silicon calculated with atomic cross sections, assuming: forward (red dashed line), isotropic (green dotted line), and anisotropic (Eq. (3), blue solid line) scattering.

energies the anisotropic scattering mostly occurs in forward direction, whereas for lower energies the scattering becomes more isotropic. This result qualitatively confirms a correct implementation of the scattering algorithm.

Next, we study the influence of the effective energy gap on the electron ranges. Fig. 6 compares the electron ranges in silicon calculated with atomic binding energies (grey dashed line with circles), the binding energies corrected using the effective energy gap of 1.79 eV (blue solid line with the circles), and the data from X-ray Data Booklet[27] (black solid line). The log-scale plot demonstrates an overall improvement of the agreement between the data from Ref.[27] and our theoretical electron ranges when the effective energy gap approach was used – in comparison to those obtained with atomic energy levels.

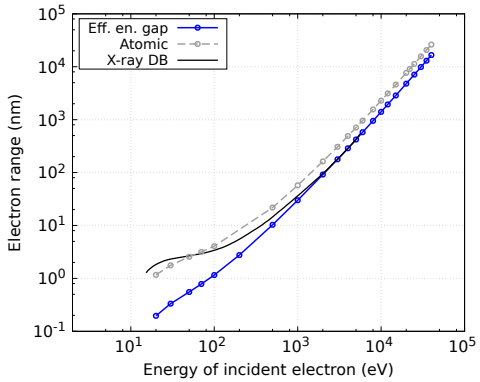

Figure 6. Electron ranges in silicon calculated with XCascade-3D using only atomic levels (grey dashed line with circles) and using the effective energy gap correction for the valence levels (solid blue line with circles). The results are compared with the predictions from the X-ray Data Booklet[27] (black solid line).

5. COMPARISON WITH OTHER DATA

Below we show our calculations of electron ranges in three materials: silicon (with the density of 2.33 g/cm^3), polystyrene (1.05 g/cm^3), and gold (19.32 g/cm^3). Fig. 7 demonstrates a good agreement between XCascade-3D predictions (blue lines with circles) and the data from X-ray Data Booklet[27] (black solid lines). Brown dotted lines are the calculations made with another code TREKIS[28] for

the same stopping threshold for electron cascading (10 eV). TREKIS uses inelastic scattering cross sections based on complex dielectric function to obtain the energy loss function. Integration of its inverse value yields the electron range. At low electron energies it is sensitive to a choice of the low-energy integration limit, which results in a shift to the entire curve. One can see that the XCascade-3D predictions are in a good agreement with both data-sets at high electron impact energies. As we mentioned above, this can be expected, since we use atomistic approximation. At lower energies the agreement worsens, but stays reasonable. In particular, the results also confirm that the calculations of electron ranges via integration of the loss function coincide well with the Monte Carlo simulation results, cross-checking the accuracy of both schemes.

With these tests, the accuracy of our new tool has been confirmed.

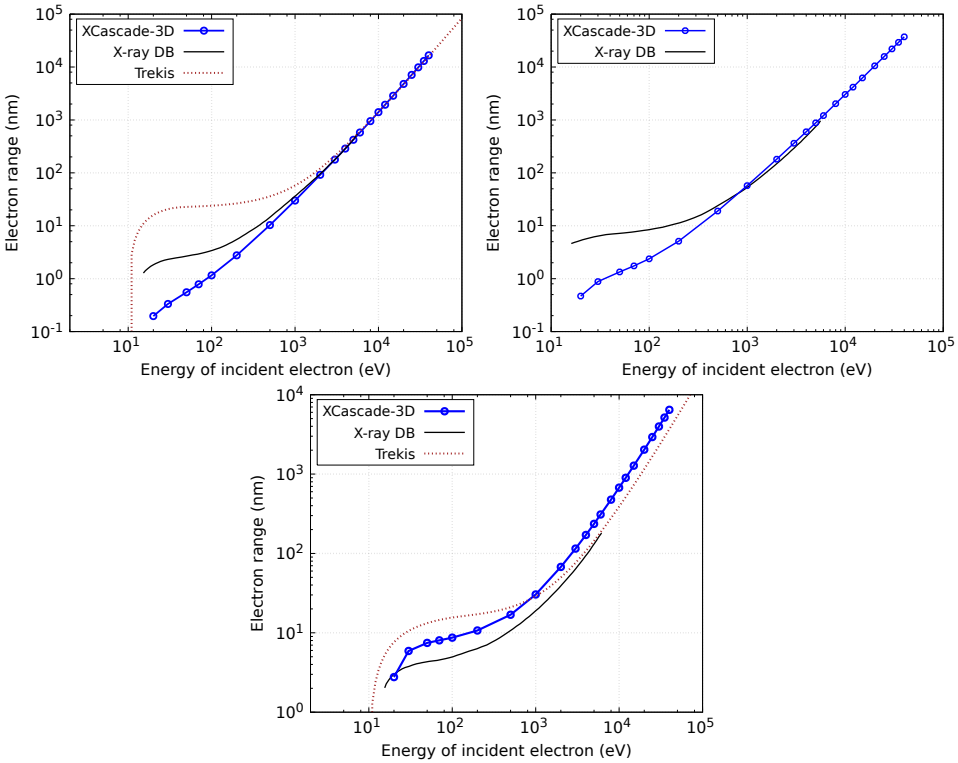

Figure 7. Electron ranges in silicon (upper left), polystyrene (upper right), and gold (below) calculated with XCascade-3D model (blue solid line), X-ray Data Booklet[27] (brown dashed line), and the simulation tool TREKIS.[28]

6. CONCLUSION

We presented the XCascade-3D, a new Monte Carlo tool to study electron trajectories and collisional ionization events after X-ray irradiation in various materials at low irradiation fluence. We demonstrated that our parametrization of an effective energy gap (wherever applicable) improves the results in comparison with simulations with purely atomic binding energies. Our calculations show a good agreement of the electron ranges with the results of previously published model TREKIS and with the X-ray Data Booklet data for silicon, gold, and polystyrene. The code is now ready for quantitative applications in the context of diagnostics of XFEL pulses.

ACKNOWLEDGMENTS

Authors thank S. Pikuz and S.-K. Son for helpful discussions.

REFERENCES

[1] Ziaja, B., London, R. A., and Hajdu, J., "Unified model of secondary electron cascades in diamond," *Journal of Applied Physics* **97**(6), 064905 (2005).

[2] Ackermann, W., Asova, G., Ayvazyan, V., Azima, A., Baboi, N., Bähr, J., Balandin, V., Beutner, B., Brandt, A., Bolzmann, A., et al., "Operation of a free-electron laser from the extreme ultraviolet to the water window," *Nature Photonics* **1**(6), 336–342 (2007).

[3] Emma, P., Akre, R., Arthur, J., Bionta, R., Bostedt, C., Bozek, J., Brachmann, A., Bucksbaum, P., Coffee, R., Decker, F.-J., et al., "First lasing and operation of an ångstrom-wavelength free-electron laser," *Nature Photonics* **4**(9), 641–647 (2010).

[4] Pile, D., "X-rays: First light from sacla," *Nature Photonics* **5**(8), 456 (2011).

[5] Allaria, E., Appio, R., Badano, L., Barletta, W., Bassanese, S., Biedron, S., Borga, A., Busetto, E., Castronovo, D., Cinquegrana, P., et al., "Highly coherent and stable pulses from the fermi seeded free-electron laser in the extreme ultraviolet," *Nature Photonics* **6**(10), 699–704 (2012).

[6] Altarelli, M., Brinkmann, R., Chergui, M., Decking, W., Dobson, B., Dsterer, S., Grbel, G., Graeff, W., Graafsma, H., Hajdu, J., Marangos, J., Pflger, J., Redlin, H., Riley, D., Robinson, I., Rossbach, J., Schwarz, A., Tiedtke, K., Tschentscher, T., Vartaniants, I., Wabnitz, H., Weise, H., Wichmann, R., Witte, K., Wolf, A., and Wulff, M., "The european x-ray free-electron laser," *The European X-Ray Free-Electron Laser Technical Design Report, DESY XFEL Project* **97**, 1–26 (2007).

[7] Norman, G., Starikov, S., Stegailov, V., Fortov, V., Skobelev, I., Pikuz, T., Faenov, A., Tamotsu, S., Kato, Y., Ishino, M., et al., "Nanomodification of gold surface by picosecond soft x-ray laser pulse," *Journal of Applied Physics* **112**(1), 013104 (2012).

[8] Stern, S., Holmegaard, L., Filsinger, F., Rouzée, A., Rudenko, A., Johnsson, P., Martin, A. V., Barty, A., Bostedt, C., Bozek, J., et al., "Toward atomic resolution diffractive imaging of isolated molecules with x-ray free-electron lasers," *Faraday Discussions* **171**, 393–418 (2014).

[9] Medvedev, N., "Femtosecond x-ray induced electron kinetics in dielectrics: application for fel-pulse-duration monitor," *Applied Physics B* **118**(3), 417–429 (2015).

[10] Riedel, R., Al-Shemmary, A., Gensch, M., Golz, T., Harmand, M., Medvedev, N., Prandolini, M., Sokolowski-Tinten, K., Toleikis, S., Wegner, U., et al., "Single-shot pulse duration monitor for extreme ultraviolet and x-ray free-electron lasers," *Nature Communications* **4**, 1731 (2013).

[11] Harmand, M., Coffee, R., Bionta, M. R., Chollet, M., French, D., Zhu, D., Fritz, D., Lemke, H., Medvedev, N., Ziaja, B., et al., "Achieving few-femtosecond time-sorting at hard x-ray free-electron lasers," *Nature Photonics* **7**(3), 215–218 (2013).

[12] Baldacchini, G., Bollanti, S., Bonfigli, F., Flora, F., Di Lazzaro, P., Lai, A., Marolo, T., Montereali, R., Murra, D., Faenov, A., et al., "Soft x-ray submicron imaging detector based on point defects in lif," *Review of Scientific Instruments* **76**(11), 113104 (2005).

[13] Pikuz, T., Faenov, A., Matsuoka, T., Matsuyama, S., Yamauchi, K., Ozaki, N., Albertazzi, B., Inubushi, Y., Yabashi, M., Tono, K., et al., "3d visualization of xfel beam focusing properties using lif crystal x-ray detector," *Scientific Reports* **5** (2015).

[14] Jacoboni, C. and Reggiani, L., "The Monte Carlo method for the solution of charge transport in semiconductors with applications to covalent materials," *Reviews of Modern Physics* **55**(3), 645 (1983).

[15] Ziaja, B. and Medvedev, N., "Modelling ultrafast transitions within laser-irradiated solids," *High Energy Density Physics* **8**(1), 18–29 (2012).

[16] Medvedev, N. and Rethfeld, B., "Effective energy gap of semiconductors under irradiation with an ultrashort VUV laser pulse," *EPL (Europhysics Letters)* **88**, 55001 (dec 2009).

[17] Cullen, D. E., Hubbell, J. H., and Kissel, L., [*EPDL97: the Evaluated Photon Data Library, '97 version.*], Lawrence Livermore National Laboratory, UCRL–50400, Livermore, CA, vol. 6, re ed. (1997).

[18] Perkins, S., Cullen, D., Chen, M., Rathkopf, J., Scofield, J., and Hubbell, J., "Tables and graphs of atomic subshell and relaxation data derived from the llnl evaluated atomic data library (eadl), z= 1–100," tech. rep., Lawrence Livermore National Lab., CA (United States) (1991).

[19] Keski-Rahkonen, O. and Krause, M. O., "Total and partial atomic-level widths," *Atomic Data and Nuclear Data Tables* **14**(2), 139–146 (1974).

[20] Ziaja, B., Jurek, Z., Medvedev, N., Thiele, R., and Toleikis, S., "A review of environment-dependent processes within FEL excited matter," *High Energy Density Physics* **9**, 462–472 (2013).

[21] Kim, Y.-K. and Rudd, M. E., "Binary-encounter-dipole model for electron-impact ionization," *Physical Review A* **50**(5), 3954 (1994).

[22] Plante, I. and Cucinotta, F. A., "Cross sections for the interactions of 1 ev–100 mev electrons in liquid water and application to monte-carlo simulation of hze radiation tracks," *New Journal of Physics* **11**(6), 063047 (2009).

[23] Jenkins, T. M., Nelson, W. R., and Rindi, A., [*Monte Carlo transport of electrons and photons*], vol. 38, Springer Science & Business Media (2012).

[24] Okhrimovskyy, A., Bogaerts, A., and Gijbels, R., "Electron anisotropic scattering in gases: A formula for monte carlo simulations," *Physical Review E* **65**(3), 037402 (2002).

[25] Medvedev, N. and Rethfeld, B., "Transient dynamics of the electronic subsystem of semiconductors irradiated with an ultrashort vacuum ultraviolet laser pulse," *New Journal of Physics* **12**, 073037 (jul 2010).

[26] Alig, R. and Bloom, S., "Electron-hole-pair creation energies in semiconductors," *Physical Review Letters* **35**(22), 1522 (1975).

[27] Thompson, A., Attwood, D., Gullikson, E., Howells, M., Kortright, J., Robinson, A., et al., "X-ray data booklet (2009)," *URL http://xdb. lbl. gov* (2009).

[28] Medvedev, N., Rymzhanov, R., and Volkov, A., "Time-resolved electron kinetics in swift heavy ion irradiated solids," *Journal of Physics D: Applied Physics* **48**(35), 355303 (2015).